Arch. Min. Sci. **70** (2025), 1, 85-100

Electronic version (in color) of this paper is available: http://mining.archives.pl

DOI: https://doi.org/10.24425/ams.2025.154164

ŁUKASZ KAPUSTA[1*], LESZEK SZOJDA[2]

# ANALYSIS OF THE DEFORMATION OF TRADITIONAL MULTI-STOREY RESIDENTIAL BUILDINGS CAUSED BY THE CURVATURE OF THE TERRAIN – CASE OF STUDY

Knowledge of the relationship between the curvature of the terrain and the curvature of the building can be a significant factor in assisting the process of introducing building prophylaxis for existing residential buildings made of traditional technology. Every year, a significant proportion of the costs resulting from the mining damage is spent on repairs to such buildings. In this study, the relationship between the curvature of the terrain and the curvature of two four-storey traditional residential buildings was determined. To this purpose, surveying was carried out for the two selected buildings and the terrain area near the buildings. This allowed us to describe the relationship between the two curvatures. Subsequently, FEM analyses were carried out in the building-substrate system for both buildings. The relationship between the curvatures was determined by the coefficient α and displayed graphically. The determined relationship may in future be a tool to assist in the design process of building prevention solutions for similar existing structures. It must be noted though, that the analyses were limited to a single experiment. More data should be collected from other research facilities to permanently introduce similar simplification solutions into design practice.

**Keywords:** Mining subsidence; ground curvature; geodesy monitoring; numerical analysis; masonry structures

## 1. Background

Coal mining results in the formation of voids in the rock mass, which then close due to gravitational forces [1]. The ground surface above the mining site is deformed, which can re-

[1] KIELCE UNIVERSITY OF TECHNOLOGY, FACULTY OF ENVIRONMENTAL ENGINEERING, GEOMATICS AND RENEWABLE ENERGY, AL. TYSIĄCLECIA PAŃSTWA POLSKIEGO 7, 25-314, KIELCE, POLAND
[2] SILESIAN UNIVERSITY OF TECHNOLOGY, 2A AKADEMICKA STR., 44-100 GLIWICE, POLAND
* Corresponding author: kapusta.lukasz@gmail.com

sult in mining damage. According to data from the Industrial Development Agency, in the first quarter of 2024 alone, the costs of eliminating mining damage in Poland amounted to PLN 76 million. Each year, these costs amount to approximately PLN 300-400 million. Nearly 1/4 of this sum was spent on repairs to residential buildings. Every year in Poland, several thousand buildings that have suffered mining damage are renovated. There has been a significant reduction in coal mining in Poland [2,3]. In 2023, output fell below 50 million tons. However, in the same year, the world's largest coal producers set new records. Mining damage is, therefore, a significant global problem. Deformations of the ground surface can be divided into continuous and discontinuous types [1], and in practice, continuous deformations dominate [4-6]. The theory of predicting land surface deformation because of mining activities was proposed at the beginning of the 20th century. The first theory for predicting the subsidence of a mining field of any shape, based on geometric-integral relations, was proposed in the 1930s [7]. Subsequently, this theory was expanded [8,9]. In the largest coal-producing countries (China, the USA and the countries of Central and Eastern Europe, especially Poland), the theory presented in [8] is used to calculate land surface deformations. According to this, continuous surface deformations are described by five parameters: subsidence $w$, slope $T$, radius of curvature $R$ (or curvature $K = 1/R$), horizontal displacement $U$ and horizontal strain $\varepsilon$. The theoretical basis for the behaviour of building structures under these influences is given in [10], and according to its assumptions, the number of relevant soil parameters can be reduced to two: curvature $K$ and horizontal deformation $\varepsilon$.

Uneven depressions of the ground surface resulting from the emerging curvature pose a significant threat to the building structure. This is mainly because they result in dangerous deformation of the structure, which was unforeseen in the design phase [1,11-13]. It is worth mentioning that there are also several other factors which cause a similar effect. Natural phenomena may cause uneven depressions and, as a result, bending of the structures, and these include: a complex and poorly recognised structure of the ground under the foundation, changes in the properties of the ground over time and within the foundation of the building (e.g. due to changes in soil and water relations), and mass movements in the form of landslides. The second group includes deformations related to human activity, e.g. the formation of excavations or tunnels in areas of dense urban development [14] and all works related to the exploitation of deposits. It should be added that the closure of mines and the cessation of mining are associated with the flooding of workings, which may be accompanied by elevation of the ground surface, resulting in deformations [15].

Buildings, particularly at risk of uneven ground depressions, are those constructed using traditional technologies, specifically brick buildings from the 19th and 20th centuries, which were built before the start of underground mining. Such structures account for a significant portion of the total cost associated with mitigating mining damage. Fig. 1 shows the potential cracking of the masonry structure of a building constructed with traditional technology for a convex curvature.

It is known that, theoretically, the deformation of the subsoil-building system depends on a building's geometry. Building deformations also hinge on the stiffness of the structure. If buildings had zero stiffness, they would faithfully reflect the deformations of the mining ground. On the other hand, if objects had infinite stiffness, they would not deform due to the deformation of the ground. We are dealing with an intermediate value. Building structures bend differently from the ground surface. If we denote the curvature of the terrain as $K$ and the curvature of an object as $K^*$, then such an object will be affected by a certain resultant curvature [1].

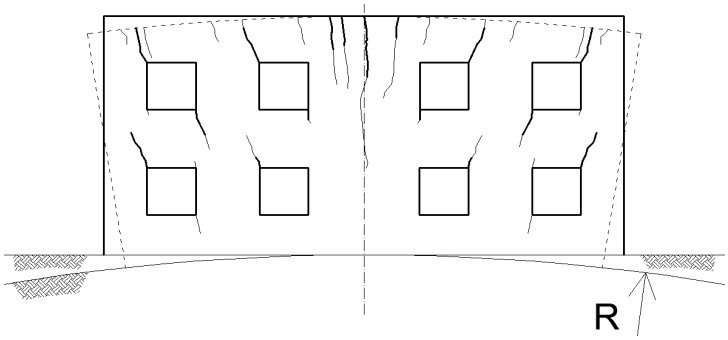


Fig. 1. Damage to building wall structure caused by convex curvature (*source:* own work based on [1])

Assuming that the curvatures $K$ and $K^*$ are proportional and that they are of the same sign due to the mechanics of the phenomenon, there is a relationship between them

$$\alpha = \frac{K^*}{K} \tag{1}$$

where: $\alpha$ – coefficient determining the deformability of the object.

The Polish guidelines [17] propose a procedure for calculating the equivalent flexural rigidity $EJ_{zast}$ [18] which consists of the modulus of elasticity (Young's) $E$ of the material and the moment of inertia of the element cross-section $J$. According to this procedure, the equivalent area moment of inertia of the building wall is determined according to the formula:

$$J_{zast} = \frac{(0.5L)^2}{\sum_{i=1}^{n} \frac{a_i \cdot x_i}{J_i}} \tag{2}$$

where:

$a_i, x_i$ – values adopted in accordance with Fig. 2,

$J_i$ – moment of inertia of the wall cross-section (in the $i$ cross-section) determined based on formula (3)

$$J_i = \sum \left[ \frac{b_{i,j} h_{i,j}^3}{12} + F_{i,j} \left( z_{i,j} - \overline{z}_i \right)^2 \right] \tag{3}$$

where:

$F_{i,j}$ – cross-sectional area for the $j$-th element in the cross-section of the $i$-th element section,

$b_{i,j}, h_{i,j}$ – cross-sectional dimensions of the $j$-th element in the cross-section of the $i$-th element section,

$z_{i,j} - \overline{z}_i$ – distance (in the vertical direction) between the $i$-th centre of gravity of the cross-section of the element and the centres of gravity of the $j$-th components of the cross-section of the element.

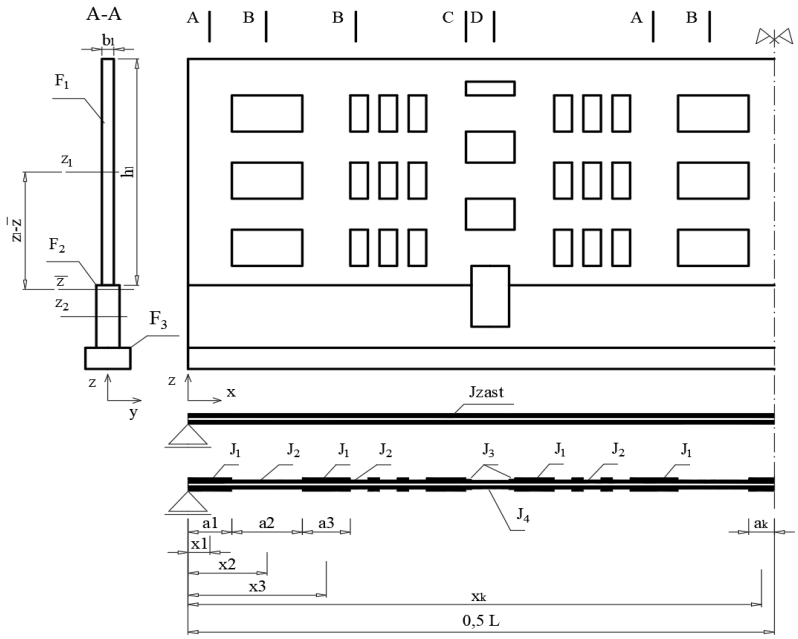


Fig. 2. Scheme for calculating the equivalent moment of inertia of the wall (*source:* own work based on [17])

The flexural rigidity of the longitudinal wall [17] is:

$$EJ_{zast} = \kappa EJ_{zast} \tag{4}$$

where:

$\kappa$ – 0.8 (monolithic wall), coefficient determined empirically, adopted for calculations based on [17]

$$E = 0.7E_b$$

$E_b$ – modulus of elasticity.

From the perspective of structural mechanics, the interaction of the building with the deforming ground is one of the most challenging and complex problems [1,17,19-21], including the field of numerical modelling of preventive solutions [22,23]. Simplified analyses of a building on a curved base are now being replaced by FEM computer modelling because of their 'approximate' nature. In engineering practe, the impact of ground deformation on buildings is implemented as a spatial shell model of a building on elastic ground [24-27]. More advanced computational models are characterised by an elastic-plastic model of the structure and the substrate [28-29]. Currently, work is also being carried out on an advanced computational approach to assessing the risk of damage to buildings subject to negative kinematic impacts of underground mining using tools from artificial intelligence methods [30,31].

Numerical modelling of building structures using calculation programs often involves assuming unambiguous values of loads or displacements. In the case of mining areas, it is crucial to

introduce actual values of interactions (e.g., the curvature of the object), which are not the values of the deforming terrain not burdened with the object-terrain curvature. Knowledge of the value of the $\alpha$ coefficient (1) could be a crucial factor supporting numerical modelling. In this paper, an attempt was made to determine the value of the $\alpha$ coefficient for buildings selected for research. The adopted objects are examples of typical, traditional, existing urban development. Buildings of this type are particularly exposed to the influence of terrain curvature because they were not designed to safely transfer loads caused by the curvature of the mining area and, in many cases, require appropriate construction prevention.

## 2. Characteristics of the research facility

Mining areas provide a good experimental field for testing the association of a building with the deforming ground [1]. Thanks to the knowledge of the location of the exploited seam and the ability to predict ground deformation, it is possible to prepare a measuring observation polygon for examining the relationship between the curvature of the terrain and the building [32-34].

The field research presented in this work was carried out in Bytom. In this case, many years of multi-deck exploitation have caused depressions reaching over 20 meters over the last sixty years [12]. The effect of such intensive mining activity can now be seen based on GIS databases, generating a comparison of digital terrain models over the years [35-37]. Fig. 3, prepared in the Q-Gis Program, shows a comparison of digital terrain models (DTM) from 2001-2021. The zones marked in blue with blurred contours constitute a post-exploitation depression basin.

The location of the residential estate of traditional multi-storey residential buildings studied is marked with a red ellipse. Part of this development is the subject of our analysis. A total of two buildings were selected:

- Object A – a single segment, 44.3 m long and 10.8 m wide,
- Object B – two-segments with segment dimensions of: 12.7×11.8 m and 17.8×10.9 m.

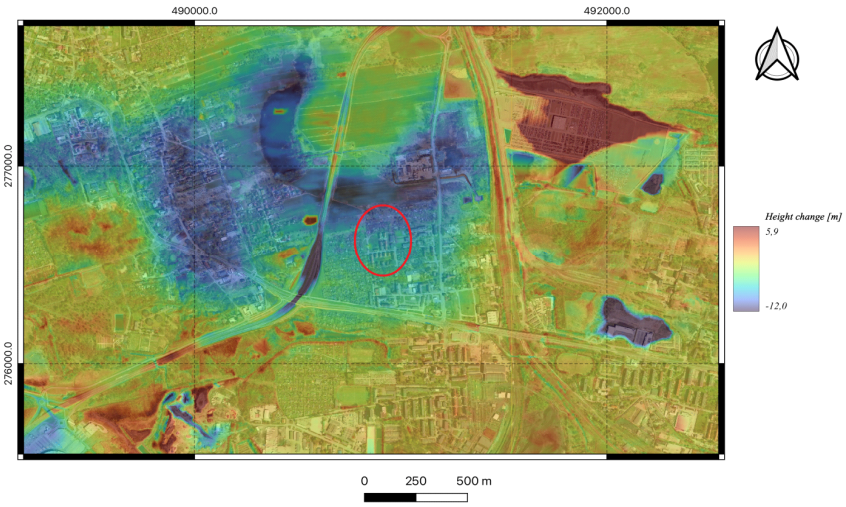


Fig. 3. DTM comparison result for 2001:2021

All the objects had similar construction details, three-storey buildings from the 1920s, made using traditional brick technology. The ceilings above the basement were made using the Klein technology and the rest are wooden. The buildings were often located in the zone of active mining activity (Fig. 4). In 2014-2016, a 1.8 m thick mining front wall ran directly beneath them, at approximately 710 m. It was located perpendicular to their longer edges. The location of the analysed buildings (regarding the exploited field) and the progressive exploitation over time are shown in Fig. 5.

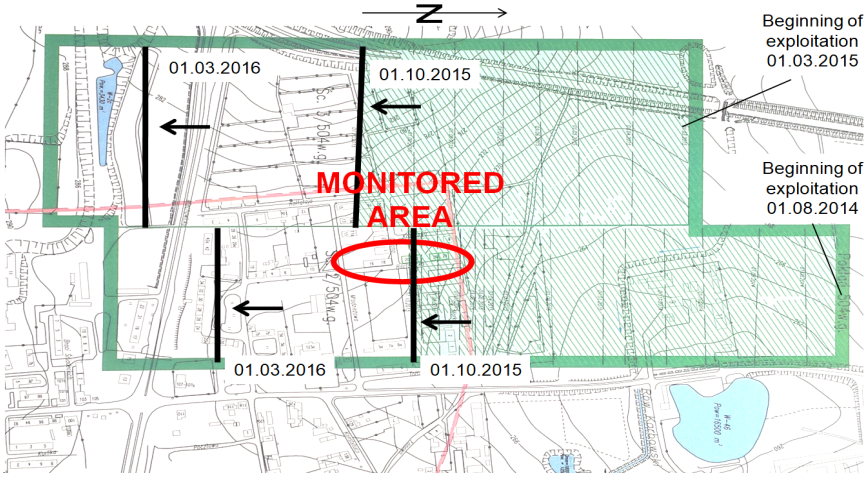


Fig. 4. Location of the building in relation to the exploitation field and exploitation progress over time (*source:* own work)

During the passing of the mining front, measurements of the curvature of the terrain and the curvature of the buildings were carried out simultaneously. The curvature of the terrain was measured on a ground line parallel to the longer, southern walls of both buildings (Figs. 5 and 6). In turn, the curvature of the buildings was measured on the southern external walls, parallel to the ground line.

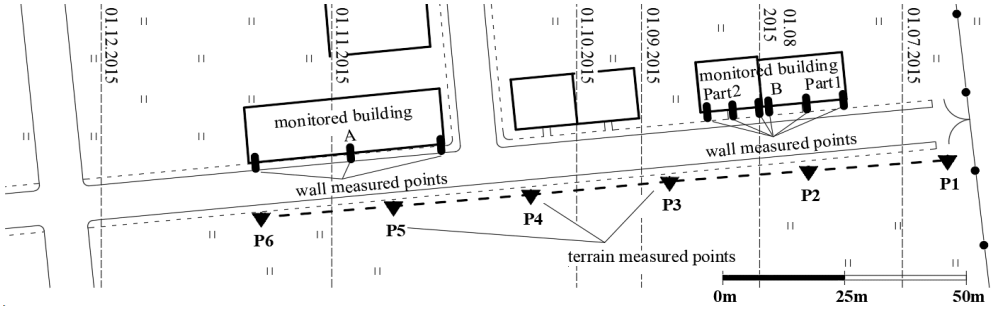


Fig. 5. Location of the field line in relation to the monitored buildings (*source:* own work)

Fig. 6. View of the street along which the field measurement line P1-P6 was stabilised. Building A is visible in the background

## 3. Results of field measurement

Cyclic levelling measurements allowed for capturing changes in the inclination of individual sections between field and wall benchmarks. The Sokkia SDL 50 code level was used for the measurements. The accuracy of the instrument is defined as the standard deviation for 1 km of double-levelling and is ±1.5 mm. The approximate value of the curvature of the terrain and the building was determined based on the formula:

$$K_i = \frac{N_{li} - N_{l(i+1)}}{l_{av}} \tag{5}$$

where:

$N_{li}$ – slope for section $l_i$,

$l_{av}$ – average length of two sections meeting at the point for which the curvature was determined.

Fig. 7 shows the relationship between the curvature of buildings A and B (Segments 1 and 2) in relation to the curvature of the terrain at the nearest points of the terrain line.

The graph in Fig. 7 shows that similar convex curvature results were obtained at field points 2 and 5. At point P2, the maximum curvature appeared earlier, which is consistent with the direction of exploitation. The greatest curvature of the structure was observed for building A. In turn, the curvatures of individual segments of building B were much smaller. Determining the curvature using geodetic techniques for short, several-meter-long deep-beams based on monitoring changes in the slopes of sections connecting adjacent wall benchmarks is subject to significant measurement error. The curvature determined on the basis of changes in the inclination of sections between wall benchmarks located at a distance of several metres, measured using geometric levelling, is determined with a much lower accuracy than in the case of longer sections [11]. In the analysed case, the measurement errors mentioned above were visible in the unstable nature of the graphs for both segments of building B: thin line: blue and green. The distance between the

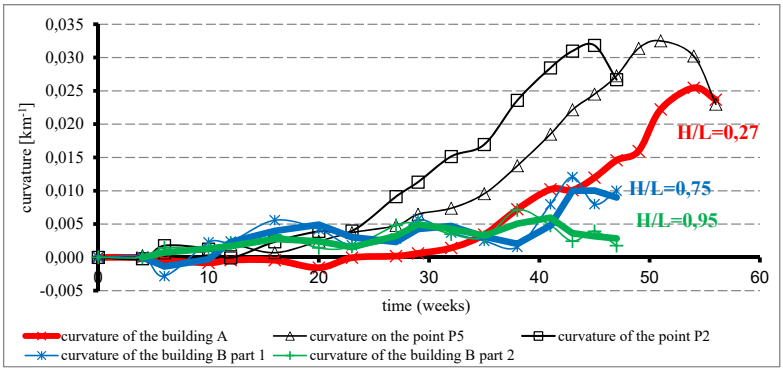


Fig. 7. Results of field measurements showing the relationship between the curvature of the terrain and buildings (*source:* own work)

wall benchmarks in this case was several meters. By introducing trend lines to the graph (thick line: blue and green – Fig. 7) it is possible to show average, approximate results, gaining in readability. For longer measurement sections, the course of the graph has a much milder character, which suggests a significantly smaller contribution of error to the obtained results. Both in the measurements of terrain curvature (black lines – Fig. 7) and for building A (red line – Fig. 7), the distances between the benchmarks were significantly longer (approx. 20-25 m).

The curvature of the buildings presented in the graph was determined in the longitudinal direction, parallel to the terrain line. During field measurements, changes in the curvature of the western gable wall of building A were also measured in the same way, in the transverse direction. The results of geodetic measurements did not show, in this case, significant changes in the curvature, therefore only the curvature in the longitudinal direction was considered in further analyses.

The ratio of the curvature of the terrain and the building in the longitudinal cross-section obtained from field measurements, in the case of the tested objects, is strongly dependent on the $H/L$ value, i.e. the ratio of the height to the length of the bent walls. Buildings A and B are very similar, in terms of construction, and have similar stiffness. Nevertheless, building A responded much more strongly to the appearance of terrain curvature than the shorter segments of building B.

## 4. Numerical model of buildings

The next stage of examining the relationship between the curvature of the terrain and the selected buildings was FEM numerical analysis. The buildings were modelled as three-dimensional shell objects resting on elastic ground. The material properties were defined as linear elastic. Such computational models are widely used in engineering practice and are in line with the guidelines [17]. The material parameters adopted for the analyses were based on macroscopic tests for expert opinions commissioned by the mine (TABLE 1).

The analysis did not consider wooden floors or the roof, due to the negligible stiffness of these types of elements. They do not constitute an important element in the reinforcing of bending walls [11]. All building dimensions and wall thicknesses were adopted based on the author's inventory. The thickness of the basement walls was 52 cm, and the remaining floors were 38 cm, respectively. The building plans are shown in Fig. 8.

TABLE 1

Material parameters assumed in the numerical analyses (based on classified materials from the Mining Plant)

| Material parameter | Units | Value | |
|---|---|---|---|
| Compressive strength | $f_k$ [MPa] | 2.2 | Masonry |
| Weight by volume | $\gamma$ [kN/m$^3$] | 18 | |
| Modulus of elasticity | $E$ [MPa] | 910 | |
| Degree of plasticity | $I_L$ [-] | 0.2 | Soil |
| Angle of internal friction | $\phi$ [°] | 18 | |
| Cohesion | $c$ [kPa] | 32 | |

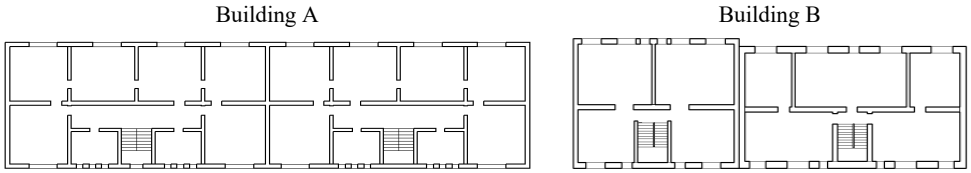


Fig. 8. Projections of the repeating floors of the monitored buildings (*source:* own work)

The terrain curvature model was constructed according to the national guidelines [20], which allow for the application of curvature to the building model in the form of forced vertical displacements, imposed in elastic support nodes imitating the ground. For both buildings (A and B), the maximum terrain curvature was modelled with a radius corresponding to the results of geodetic measurements and, therefore, consistent with the actual deformations of the ground. The value of the applied curvature in the models of the buildings equals the maximum values measured in the field (Fig. 7 – black lines). The curvature (radius $R$ = 31.4 km) measured from benchmark no 2 was imposed on the models of both segments of the building B – Fig. 5. The curvature (radius $R$ = 30.8 km) measured from benchmark no 5 was imposed on the model of the building A – Fig. 5. The calculations were performed using Autodesk Robot Structural Analysis Professional 2024 software and the computational model is shown in Fig. 9.

Although in practice the curvature of the terrain was accompanied by horizontal deformations that were the subject of field measurements, they were not considered in the modelling. Considering the horizontal tensile strains at the foundation level had no significant effect on the amount of deflection of the modelled structures [11].

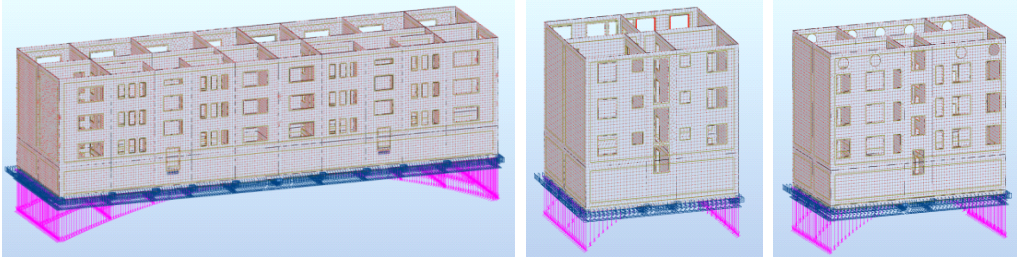

Fig. 9. Computational models of buildings A and B adopted for the analysis (*source:* own work)

## 5. Results of numerical calculations

For the computational models presented in Fig. 9, stiffness was estimated in accordance with the guidelines presented in (2) and (4). First, the moments of inertia were determined for the longitudinal bending walls of buildings. The procedure for determining the stiffness of the entrance wall of Building A is presented in detail below.

In the cross-sections marked in Fig. 2, the moments of inertia were determined according to (3):

$$J_{A\text{-}A} = 80.3 \text{ m}^4$$
$$J_{B\text{-}B} = 60.7 \text{ m}^4$$
$$J_{C\text{-}C} = 66.4 \text{ m}^4$$
$$J_{D\text{-}D} = 61.0 \text{ m}^4$$

Then, the equivalent moment of inertia $J_{zast}$ of the wall was determined according to (2), in accordance with [17]. The values of flexural rigidity calculated from formula (4) for the longitudinal walls of the analysed building are listed below:

- flexural rigidity for the entrance wall: $EI_{zast} = 35\ 220$ MN m$^2$.

In the same way, the flexural rigidity was determined for the remaining longitudinal walls:

- flexural rigidity for the internal wall: $EI_{zast} = 38\ 996$ MN m$^2$,
- flexural rigidity for the rear wall: $EI_{zast} = 35\ 384$ MN m$^2$.

After summing the flexural rigidity of all the longitudinal walls, the final stiffness for the entire building is: $EI_{zast\ for\ the\ building} = 109\ 600$ MN m$^2$. Similar calculations were also made for the individual segments of Building B. In this case, the variable element in the computational analyses was the modulus of elasticity of the walls: 910 MPa, 2 GPa, 3 GPa, 4 GPa, 5 GPa and 10 GPa.

Fig. 10 shows the relationship between the curvatures of the models of Building A and Building B and the curvature of the terrain, with the variable stiffness of longitudinal bending walls.

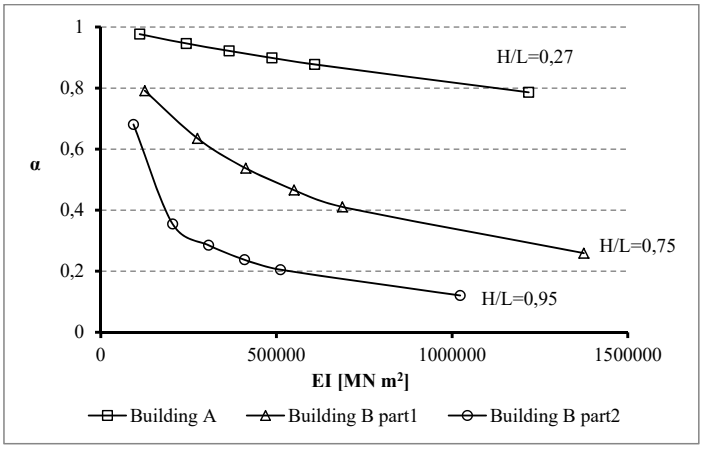


Fig. 10. Diagram of the $\alpha$ coefficient with variable stiffness of the tested buildings (*source:* own work)

The graph shows that building model A was bent the most. Segments 1 and 2 of building B obtained a smaller curvature with very similar terrain curvatures applied to the models. This confirms the relationship observed in the field measurements. It should be noted that, in the case of a change in stiffness, greater discrepancies in the α coefficient are observed for buildings with a larger $H/L$ ratio. Building A has a $H/L$ ratio of 0.27 and the variability of the $\alpha$ coefficient is smaller in this case. For objects with higher $H/L$ ratios, the $\alpha$ coefficient variability diagram is curvilinear. Fig. 11 shows the level of principal stresss1 for the facade walls of buildings A and B for the initial variant ($E$ = 910 MPa). In the calculation program used for the analyses, the main tensile stress $s1$ in the finite element is defined by (6).

$$s1 = \frac{sXX + sYY}{2} + \sqrt{\frac{\left(sXX - sYY\right)^2}{4} + sXY^2} \tag{6}$$

The obtained stress maps show that the terrain curvature measured in the field tests poses the greatest threat to Building A. It is worth mentioning that Building A began to crack when the maximum terrain curvature occurred (Fig. 12). A detailed analysis of the object's cracks was presented in [38].

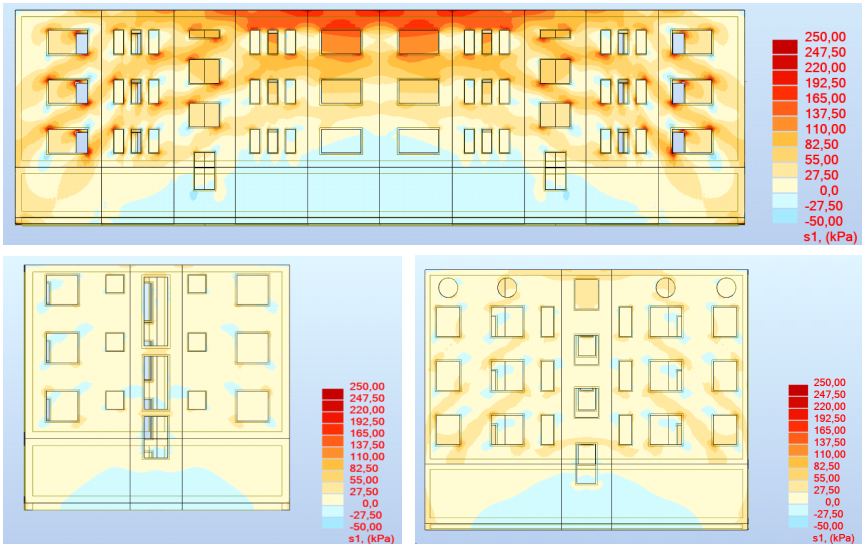


Fig. 11. Stress distribution maps of s1 for buildings A and B: segments 1 and 2 (*source:* own work)

Segments 1 and 2 of Building B were not damaged when the maximum ground curvature was revealed. The level of principal stress presented in Fig. 11 partially explains the nature of the $\alpha$ coefficient variability diagram in Fig.10. A building with a lower $H/L$ ratio is much more susceptible to bending. In the analysed case, the object bent the most out of all the tested buildings. Therefore, the stresses caused by curvature increased to dangerous levels. Objects with a higher $H/L$ ratio are less susceptible to terrain curvature and, therefore, the level of stress caused by terrain curvature is lower in this case. Similar numerical analyses are presented in [39]. The

Fig. 12. Vertical cracking in the central part of the facade wall of Building A (*source:* own work)

results obtained in that work also indicated that the values of internal forces in bending walls are strongly correlated with the length of the building.

In the second calculation step, the variables for buildings A and B were ground conditions. The stiffness of the buildings is constant in this comparison and assumed to be $E = 910$ MPa. The foundation conditions are variable. When performing numerical analyses in which the soil is reduced to the Winkel analogue, the key issue is to determine the elasticity coefficient of the substrate [17]. Autodesk Robot Structural Analysis software is based on Businesqua theory. The elasticity of the supports modelled in the model, in addition to the elasticity coefficient of the substrate, also depends on the foundation surface represented by a given support. For the base model in which the substrate is clay, $I_L = 0.2$ for the longitudinal, central footing of Building A with a width of 1.0 m $K_z = 28.3$ MN/m. For the remaining benches with a width of 0.8 cm, $K_z = 23.4$ MN/m. The $K_z$ coefficient values were obtained using the soil calculator of the software used. Then, calculations were made for buildings A and B with different soil variants. The variable ground conditions adopted for the analyses are presented in TABLE 2.

TABLE 2

Ground conditions used for the analyses

| **Type of soil** | **$E_0$ [MPa]** | **$K_z$ (average) MN/m** | | |
|---|---|---|---|---|
| | | **Building A** | **Building B (part 1)** | **Building B (part 2)** |
| Gravel | 130.5 | 77.7 | 73.4 | 73.7 |
| Thick sand | 58.4 | 37.5 | 35.1 | 35.4 |
| Clay (base) | 30.0 | 25.6 | 27.8 | 27.9 |
| Compact sandy clay | 25.1 | 16.6 | 15.5 | 15.7 |
| Dusty loam | 13.6 | 13.0 | 12.0 | 13.2 |

The variability of the $\alpha$ coefficient depends on the ground conditions for the analysed buildings and is shown in Fig. 13.

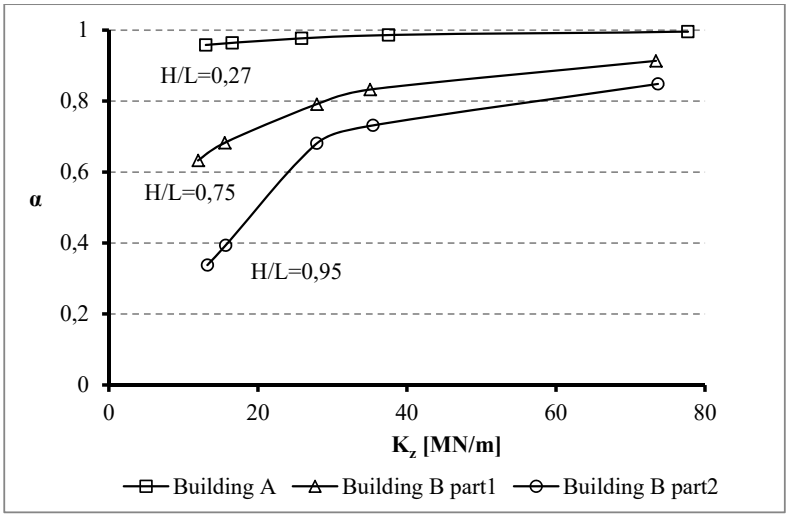


Fig. 13. Diagram of the $\alpha$ coefficient under variable foundation conditions (*source:* own work)

The graph shows that ground conditions also influence the variability of the $\alpha$ coefficient, but this influence is smaller than in the case of variable structural stiffness (Fig. 10). It is worth mentioning that the range of diversity of the adopted ground conditions is wide. Despite this, the changes in the $\alpha$ coefficient are not large. For Building A, the modelled soil subgrade does not change the $\alpha$ coefficient, which means that the adopted soil type is of secondary importance in this model. The value of the $\alpha$ coefficient for building models 1B and 2B is, indeed, sensitive to the assumed ground conditions but its large variability is only noticeable in the case of weak soil.

## 6. Conclusions

The examined relationship between the curvature of the terrain and selected buildings, constructed using traditional technology, depends on many variables. The most important factor determining the amount of bending of the structure is the $H/L$ ratio, which describes the geometry of the bent walls. The conducted research, both in the field and by calculations, shows that the ratio of the height to the length of the building's bending walls is a factor that determines the amount of deflection of the structure and the nature of the cooperation of the building with the deforming ground. Despite the similar stiffness of the tested buildings, the object with a lower $H/L$ ratio responded to the applied terrain curvature to a much greater extent, both in terms of structural deformation and stress increase. It can therefore be concluded that, in the case of buildings with similar heights of bending walls, the decisive factor which increases the risk of dangerous bending is the length of the contact zone of the wall with the curved ground; the longer it is, the greater the risk of stress increase.

Based on the numerical analyses performed (30 cases in total), it can be seen that the variability of the $\alpha$ coefficient defined in this work, defining the ratio of the curvature of the building and the ground, is more dependent on the stiffness of the building than on the ground conditions.

Based on the developed computational models, an image of the change in the value of the $\alpha$ coefficient was obtained, which may be useful in estimating the curvature of the building for the terrain curvature known from measurements or forecasts. Of course, this applies to structures with a similar shape and similar material parameters.

In the FEM models presented in this paper, a greater deflection of the structure was achieved than in reality. By comparing the actual curvature of the analysed buildings with that obtained in models built based on the guidelines [17], it can be seen that the modelling results overestimate the actual deflection of the structure. This is a typical feature of the engineering computational approach, and the issue is described in detail in [40]. Therefore, the $\alpha$ coefficient developed in Figs. 10 and 13 is a safe approach when estimating the curvature of the structure.

Based on the conducted research, an image of the change in the value of the $\alpha$ coefficient describing the relationship between the curvature of both the structure and the terrain was obtained for three tested buildings with the ratio of height to length of bending walls $H/L$ = 0.27, 0.75 and 0.95. The variables in the computational models were elastic modulus for bending walls and variable soil conditions. Detailed results showing the variability of the tested coefficient $\alpha$ are presented in Figs. 10 and 13. Knowing the ratio of the terrain curvature to the building curvature allows for introducing resultant displacements into the building model based on the known terrain curvature according to the formula: $K^* = \alpha K$.

The coefficient $\alpha$ determined in this work was developed based on a single study. In order to permanently introduce similar simplifying solutions into design practice, a larger amount of data from similar research objects should be collected. Moreover, the buildings analysed in this work are built using traditional construction technology. Today's construction solutions differ from those analysed in the work. The two problems mentioned above constitute the basic limitations to the use of the value of the determined coefficient $\alpha$ on a wider scale.

## References

[1] J. Kwiatek, Construction facilities on mining areas. Wyd. GIG Katowice (in Polish), p. 266, 2007.

[2] J. Balcerowski, Z. Charkowska, In Search of Sources, Methane emissions in the Polish hard coal mining industry and the reporting system. Insrtat Policy Paper 01/2023.

[3] K. Rabiej Sienicka, T.J. Rudek, A. Wagner, Let it Flow, Our Energy or Bright Future: Sociotechnical imaginaries of energy transition in Poland. Energy Research and Social Science **89** (2022). DOI: https://doi.org/10.1016/j.erss.2022.102568

[4] Y. Jiang, R. Misa, K. Tajduś, A. Sroka, Y. Jiang, A new prediction model of surface subsidence with Cauchy distribution in the coal mine of thick topsoil condition. Archives of Mining Sciences **65** (1), 147-158 (2020). DOI: https://doi.org/10.24425/ams.2020.132712

[5] A. Sroka, S. Knothe, K. Tajduś, R. Misa, Point Movement Trace Vs. The Range Of Mining Exploitation Effects In The Rock Mass. Archives of Mining Sciences **60**, 4, 921-929 (2015). DOI: https://doi.org/10.1515/amsc-2015-0060

[6] K. Tajduś, Analysis of horizontal displacement distribution caused by single advancing long wall panel excavation. Journal of Rock Mechanics and Geotechnical Engineering **1** (4) (2015). DOI: https://doi.org/10.1016/j.jrmge.2015.03.012

[7] R. Bals, Beitrag zur Frage der Vorausberechnung bergbaulicher Senkungen. Mitteilungen aus dem Markscheidewese, Verlag Konrad Witter, Stuttgart, 1931/32.

[8] S. Knothe, Equation of the profile of the ultimately developed subsidence basin. Archiwum Górnictwa i Hutnictwa, (in Polish) **1**, 1 (1953).

[9] W. Ehrhard, A. Sauer, Die Vorausberechnung von Senkung, Schieflage und Krummung uber dem Abbau in flacher Lagerung. Bergbau-Wissenschaften, 1961.

[10] Z. Budzianowski, The effect of a curved ground on a rigid structure located in a mining area. Inżynieria i Budownictwo, (in Polish), nr 6 i 7 (1964).

[11] Ł. Kapusta, Analysis of deformation of residential buildings in mining areas. PhD thesis, Silesian University of Technology, Gliwice, Poland (in Polish), 2017.

[12] L. Szojda, Ł. Kapusta, The role of expansion joints for traditional buildings affected by the curvature of the mining area. Eng. Failure Analysis **128**, 105598, 1-14 (2021).
DOI: https://doi.org/10.1016/j.engfailanal.2021.105598

[13] D. Mrozek, M. Mrozek, J. Fedorowicz, Analysis of an effectiveness of expansion joint in the Multi-family building located by mining activities. Czasopismo Inżynierii Lądowej, Środowiska i Architektury, JCEEA **34**, 64 (2017).
DOI: https://doi.org/10.7862/rb.2017.92

[14] G. Giardina, A. Marini, M.A.N. Hendriks, J.G. Rots, F. Rizzardini, E. Giuriani, Experimental analysis of a masonry facade subject to tunnelling-induced settlement. Engineering Structures **45**, 421-434 (2012).
DOI: https://doi.org/10.1016/j.engstruct.2012.06.042

[15] M. Dudek, R. Misa, D. Mrocheń, A. Sroka, K. Tajduś, Assessment and Duration of the Surface Subsidence after the End of Mining Operations. Energies **15** (22) (2022). DOI: https://doi.org/10.3390/en15228711

[16] L. Szojda, Structural aspects of buildings protection in mining areas. Publishing House of the Silesian University of Technology, Gliwice, Monography (in Polish), 2019.

[17] Instructions, Guidelines, Guidance 416/2006. The design of buildings in mining areas, Publishing House of ITB, Warsaw (in Polish).

[18] F. Andermann, L. Fedorowicz, J. Fedorowicz, Calculation of bending long wall buildings in mining areas. Ochrona Terenów Górniczych **78**, 37-44 (in Polish), (1986).

[19] L. Fedorowicz, Contact Issues building – subsoil. Part I. Criteria of modelling and analysis of fundamental design issues contact Building – subsoil. Scientific Papers of Silesian University of Technology, Civil Engineering Series, 1729, 107, Publishing house of the Silesian University of Technology, Gliwice (in Polish), 2006.

[20] J. Fedorowicz, Contact problem of building – subsoil. Part II. The criteria for creating and evaluating computational models of system design building – ground mining. Scientific Papers of Silesian University of Technology, Civil Engineering Series, 1805, 114, Publishing house of the Silesian University of Technology, Gliwice (in Polish), 2008.

[21] Instructions, Guidelines, Guidance 364/2007, Technical requirements for buildings erected in mining areas. Publishing House ITB, Warsaw (in Polish).

[22] A. Sroka, R. Misa, K. Tajduś, M. Dudek, Analytical design of selected geotechnical solutions which protect civil structures from the effects of underground mining. Journal of Sustainable Mining **18**, 1, 1-7 (2019).
DOI: https://doi.org/10.1016/j.jsm.2018.10.002

[23] R. Misa, K. Tajduś, A. Sroka, Impact of geotechnical barrier modelled in the vicinity of a building structures located in mining area. Archives of Mining Sciences **63**, 4, 919-933 (2018). DOI: https://doi.org/10.24425/ams.2018.124984

[24] L. Szojda, Ł.Kapusta, Numerical Analysis of Buildings Located on the Edge of the Post-Mining Basin. Archives of Mining Sciences **68**, 1, 125-140 (2023). DOI: https://doi.org/10.24425/ams.2023.144321

[25] L. Słowik, Influence of the building inclination on the effort of the structure in mining exploitation conditions. Acta Scientarium Polonorum – Architectura Budownictwo **16**, 3, 155-164 (2017) (in Polish).
DOI: https://doi.org/10.22630/ASPA.2017.16.3.16

[26] L. Słowik, B. Parkasiewicz, L. Chomacki, The impact on buildings of horizontal deformation of the mining substrate of the compression nature. Materiały Budowlane **11**, 27-29 (2015) (in Polish).
DOI: https://doi.org/10.15199/33.2015.11.07

[27] L. Chomacki, B. Parkasiewicz, Numerical analysis of building sequences in Bytom-Karbie taking into account the forecasted horizontal deformations of the mining area. Przegląd Górniczy **71**, 3, 72-79 (2015)

(in Polish). https://yadda.icm.edu.pl/baztech/element/bwmeta1.element.baztech-04e8447e-b71e-4d6f-8c8a-077a94775efa?q=80c6170a-7d9f-4681-80ba-3db5b373d6e4$3

[28] D. Mrozek, M. Mrozek, J. Fedorowicz, The protection of masonry buildings in a mining area. Procedia Engineering 193, International Conference on Analytical Models and New Concepts in Concrete and Masonry Structures AMCM 2017, 184-191 (2017). DOI: https://doi.org/10.1016/j.proeng.2017.06.202

[29] L. Szojda, Ł. Kapusta, Numerical analysis of the influence of mining ground deformation on the structure of a masonry residential building. Archives of Civil Engineering **67** (2021). DOI: https://doi.org/10.24425/ace.2021.138054

[30] L. Chomacki, J. Rusek, L. Słowik, Machine Learning Methods in Damage Prediction of Masonry Development Exposed to the Industrial Environment of Mines. Energies **15** (11), 3958 (2022). DOI: https://doi.org/10.3390/en15113958

[31] L. Chomacki, J. Rusek, L. Słowik, Selected Artificial Intelligence Methods in the Risk Analysis of Damage to Masonry Buildings Subject to Long-Term Underground Mining Exploitation. Minerals **11** (9), 958 (2021). DOI: https://doi.org/10.3390/min11090958

[32] J. Ostrowski, Deformations of the mining area. AGH, Kraków, 2015 (in Polish).

[33] T. Lipecki, Assessment of measurement accuracy in the context of determined terrain deformation indices. Przegląd Górniczy **67**, 1-2, 63-67 (2011). bwmeta1.element.baztech-article-AGH8-0009-0026

[34] P. Sopata, Use of GPS-RTK method to measure the surface displacements of mining areas. Przegląd Górniczy. ISSN 0033-216X. **68**, 7, 104-109 (2012). Bibliogr. s. 109.

[35] J. Blachowski, Application of GIS spatial regression methods in assessment of land subsidence in complicated mining conditions: case study of the Walbrzych coal mine (SW Poland). Nat Hazards **84**, 997-1014 (2016). DOI: https://doi.org/10.1007/s11069-016-2470-2

[36] J. Suh, An Overview of GIS-Based Assessment and Mapping of Mining-Induced Subsidence. Applied Sciences **10** (21), 7845 (2020). DOI: https://doi.org/10.3390/app10217845

[37] A. Malinowska, R. Hejmanowski, Building damage risk assessment on mining terrains in Poland with GIS application. International Journal of Rock Mechanics and Mining Sciences **47**, (2) 238-245 (2010). DOI: https://doi.org/10.1016/j.ijrmms.2009.09.009

[38] L. Szojda, Ł. Kapusta, The influence of a variable ground curvature at the passing of an exploitation front on the technical condition of a multi-family residential building. Przegląd Górniczy **73**, 12, 63-74 (2017).

[39] A. Cincio, J. Fedorowicz, The influence of changes in the geometry of the building structure on internal forces in the walls of large-panel structures. Zeszyty Naukowe Wyższej Szkoły Technicznej w Katowicach, nr 7 (2015).

[40] L. Szojda, Ł. Kapusta, Evaluation of the elastic model of a building on a curved mining ground based on the results of geodetic monitoring. Archives of Mining Sciences **65**, 2, 213-224 (2020). DOI: https://doi.org/10.24425/ams.2020.133188